NASA

Technical Memorandum 83959

OAO–3 End of Mission Power Subsystem Evaluation

Michael Tasevoli

AUGUST 1982

National Aeronautics and
Space Administration

Goddard Space Flight Center
Greenbelt, Maryland 20771

OAO–3 END OF MISSION POWER SUBSYSTEM EVALUATION

Michael Tasevoli

August 1982

GODDARD SPACE FLIGHT CENTER
Greenbelt, Maryland 20771

OAO–3 END OF MISSION POWER SUBSYSTEM EVALUATION

Michael Tasevoli
Goddard Space Flight Center
Greenbelt, Maryland

ABSTRACT

End of mission tests were performed on the OAO–3 power subsystem in three component areas: solar array, nickel-cadmium batteries and On-Board Processor (OBP) power boost operation. Solar array evaluation consisted of analyzing array performance characteristics and comparing them to earlier flight data. Measured solar array degradation of 14.1 to 17.7% after 8 1/3 years is in good agreement with theoretical radiation damage losses. Battery discharge characteristics were compared to results of laboratory life cycle test performed on similar cells. Comparison of cell voltage profiles reveals close correlation and confirms the validity of real time life cycle simulation. The successful operation of the system in the OBP/power boost regulation mode demonstrates the excellent life, reliability and greater system utilization of power subsystems using maximum power trackers.

CONTENTS

	Page
ABSTRACT	ii
INTRODUCTION	1
Objectives	3
Methodology	4
Analysis and Results	5
Radiation Detect or Degradation	6
Main Array Degradation	6
Auxiliary Array Degradation	7
Battery Discharge Characteristics	8
On-Board Processor/Power Boost Regulation	9
CONCLUSIONS AND RECOMMENDATIONS	11
ACKNOWLEDGEMENTS	12
REFERENCES	12

TABLES

Table		Page
1	OAO–3 Nickel-Cadmium Cell Design Features	13
2	Beginning of Mission Solar Array Characteristics	14
3	End of Mission Solar Array Characteristics	15
4	OBP Power Boost Evaluation Summary	16

ILLUSTRATIONS

Figure		Page
1	Block Diagram of OAO–3 Power Subsystem	17

ILLUSTRATIONS

Figure		Page
2	OAO–3 Solar Array Paddle Arrangement	18
3	OAO–3 Solar Cell Characteristics (BOL)	19
4	Battery Charger Voltage Levels	20
5	BOL LLO Array Current vs Temperature	21
6	Normalized Short Circuit Current vs 1 MeV Electron Fluence for ohm-cm n/p Conventional Silicon Cells	22
7	OAO–3 Battery Capacity Discharge Test 1	23
8	OAO–3 Battery Capacity Discharge Test 2	24
9	OAO–3 Battery and Crane Discharge Comparisons, Pack 4c, Cell S/N 559, 15% DOD and 10°C	25
10	OBP Power Boost Evaluation, Array Power vs Sunlight Time, 900 Watt Power Limit	26
11	OBP Power Boost Evaluation, Array Voltage vs Sunlight Time, 900 Watt Power Limit	27
12	Array Current and Voltage, Shunt Regulation Mode	28
13	Battery Current and Voltage, Shunt Regulation Mode	29
14	Array Current and Voltage, Maximum Power Tracker Mode	30
15	Battery Current and Voltage, Maximum Power Tracker Mode	31
16	Array Power in Shunt Regulation vs Power Boost Modes	32

OAO–3 END OF MISSION POWER SUBSYSTEM EVALUATION

INTRODUCTION

The second and third Orbiting Astronomical Observatory (OAO) missions, launched in 1968 and 1972, respectively, and spanning more than a decade of operation, were highly successful. The power subsystems for both OAO–2 and OAO–3 (Reference 1) were similar and both performed successfully until deactivated after more than 5 and 8 years of operation, respectively. Prior to the deactivation of the OAO–3 spacecraft, a variety of end of mission tests and evaluations were performed. This report presents the results of the end of mission tests and evaluations for the power subsystem.

The simplified block diagram of the OAO–3 Power Subsystem is shown in Figure 1. The subsystem consisted of a main solar array which recharges the batteries and provides additional power to the unregulated bus during the sunlight portion of the orbit, an auxiliary array which provides bus power to spacecraft loads, three nickel–cadmium batteries operated in parallel which power the bus during eclipse, and power regulation and control units for battery charging (Reference 2).

The solar array consisted of eight co-planar solar panels as shown in Figure 2. Of these, the lower left outboard (LLO) and lower right outboard (LRO) panels formed the auxiliary array and the remaining six panels comprise the main array. In addition to the power generating circuits of the solar array, two radiation detector (RD) solar cell circuits were installed on the array as shown in Figure 2. These detectors were each connected to a 68.1 ohm load and their output voltages measured by telemetry. All the cells were 1 x 2 centimeters, 0.305 mm thick, n/p silicon solar cells with a nominal base resistivity of 2 ohm-centimeters, manufactured by Heliotek, Inc. The series-parallel configuration of the cells for the various paddles is noted in Figure 2. Each cell was individually protected by a 6 mil thick, fused silica coverglass with a MgF anti-reflective coating and a multi-layer ultraviolet reflective filter manufactured by Optical Coating Laboratory, Inc. Dow

Corning R63-489 adhesive was used to bond the glasses to the cells. Nominal beginning of life (BOL) current/voltage (I-V) curves are shown in Figure 3.

Each of the three batteries consisted of 22 series-connected, 20 ampere-hour nickel-cadmium cells, manufactured by Gulton, Inc. The three batteries were packaged into two mechanical assemblies. Each assembly contained 11 cells of each battery with the two assemblies isolated on separate thermal baseplates. The batteries had a design life of 1 year in low earth orbit with a 15 to 20% depth-of-discharge (DOD). The temperature design range was 5 to 20°C and a 35°C over-temperature thermostat protected the batteries from high temperature conditions. The batteries were charged and discharged in parallel. A more detailed description of the OAO–3 battery performance appears in Reference 1. Battery cell design details are provided in Table 1. Throughout the 8 1/3 year mission, the nickel-cadmium batteries provided trouble-free performance.

Battery depth-of-discharge has been approximately 15%, battery temperatures have remained between 5 and 10°C and battery voltage and current divergence have been within telemetry resolution.

The three batteries were charged in parallel from the Power Regulator Unit (PRU) using eight commandable, temperature compensated, battery voltage levels (Figure 4). The PRU consisted of a series of power switching transistors which are turned off and on at a fixed repetition rate. The regulator's output voltage is adjusted by varying the ratio of "on" time to the repetition rate. This duty cycle is controlled by the current through the magnetic amplifier control winding in the Power Control Unit (PCU). The control current is generated either by the battery voltage limit (BVL) controller to maintain a fixed battery voltage limit, or by the On-Board Processor (OBP) to maximize array power. As the spacecraft enters sunlight, battery charging commences either in the shunt mode where the solar array connects directly to the batteries or in the power boost mode where the PRU is under direct control of the OBP. When the charge bus reaches the voltage limit established by the BVL controller, the charge mode is changed from the shunt or the power boost mode to the regulated mode. The PRU then maintains the bus at the voltage limit. The battery

charge current tapers for the remainder of the sunlight period. In the power boost mode, the power boost routine within the OBP allows the solar array to operate at higher power level than is available when the array is clamped to the battery voltage during the initial sunlight period. This increased power level results in higher initial battery charge current and higher charge-to-discharge ampere-hour ratio. Under the direction of this subroutine, the OBP monitors array voltage and current and updates array power every 6 seconds. Based on the power calculation, the OBP through the D/A converter provides a control current to the auxiliary winding of the magnetic amplifier in the PCU. This control current varies in discrete steps to either maintain the array power at 1000 watts or track the maximum array power if it drops below 1000 watts. This operation continues until the battery voltage reaches the charger voltage limit. At this point, the OBP releases control to the BVL controller which provides an output signal to the magnetic amplifier to maintain the output of the PRU at the voltage limit for the remainder of the sunlight period (Reference 3).

Because of the successful performance, extensive life and excellent reliability of the OAO–3 power subsystem, the concept was selected for the Modular Power Subsystem (MPS) for the Multimission Modular Spacecraft (MMS) (Reference 4). In particular, the OBP power tracking mode was a forerunner to the MPS/MMS Standard Power Regulator Unit (SPRU). However, because of a chip failure in the OBP early in the mission, the power boost worker was removed and the power boost mode had never been energized during the mission. The end of mission power subsystem tests and evaluations provided a unique opportunity to obtain an increased understanding of the operation of maximum power tracking systems in degraded power subsystems. It was anticipated that, because of the commonalities of the OAO and the MMS power systems, this understanding would be especially useful. In addition, performance analysis and determination of real time degradation of the solar array and batteries were expected to provide useful information relative to existing degradation models and, perhaps lead to improved models.

Objectives

The objectives of the end of mission power subsystem tests were:

a. To acquire and analyze engineering data on total real time solar array and battery degradation after more than 8 years in low earth orbit,

b. To use this analysis in determining the validity of empirical models used for predicting array and battery lifetime and,

c. To acquire and analyze the performance data for the power subsystem operating in the power boost regulation mode.

Methodology

The test procedures used to acquire the necessary engineering data for the solar array, battery discharge and OBP/Power Boost analyses were as follows:

1. Solar Array

Solar array data including temperatures, voltages and currents were collected at 1 or 2 minute intervals for a 10 minute period starting 1 minute after entry into sunlight. For these measurements, the array orientation was normal to the sun line* and the battery voltage level was set for Level 1. This data was analyzed and compared to the earliest available data, collected on the third day of flight during orbit 46.

2. Battery Discharge Characteristics

In order to analyze end of mission battery voltage characteristics, the three 20 AH nickel-cadmium batteries were discharged in parallel over two orbits to the lowest allowable bus voltage. This was accomplished by disabling the undervoltage trip and orienting the spacecraft with the array at a high angle to the sun causing the batteries to discharge even during the sunlight period.

Initially, the batteries were fully charged at BVL-2 with a spacecraft orientation of Beta 90°.As the spacecraft entered a designated eclipse period, BVL-4 was commanded while data was collected and stored for later transmission to a ground station. During the following sunlight period, the spacecraft was slewed to Beta 122°. Real time data, which is available when the spacecraft is in contact with ground stations, was used to determine when to terminate the test. After the discharge, the spacecraft was commanded back to Beta 90° and BVL-2. Following a period of 24 hours which was sufficient to fully recharge the batteries, the same procedure was repeated. For this test the Beta angle was 124° and additional loads were added.

*The spacecraft Beta angle is the angle between the spacecraft optical axis and the earth-sun line. The angle between the spacecraft optical axis and the plane of the solar array is 33.75°. Therefore, the solar array plane is normal to the sun line at approximately Beta 56°.

3. OBP/Power Boost Regulation Mode

In order to evaluate the Power Boost Regulation Mode, the software subroutine was reloaded into the OBP. The program remained unchanged except that the array power limit was changed from 1000 watts to 900 or 1300 watts to accommodate each test phase. The initial check out phase required a spacecraft orientation of Beta 78°, BVL-1, 900 watt power limit and power system data transmitted in real time for the first 12 minutes of sunlight. Since the peak array power was determined to be greater than 900 watts at this Beta angle, the PRU under the direction of the OBP limited it to the software limit of 900 watts. The final test was performed initially with the power subsystem in the shunt mode (without the power boost enabled) at Beta 90° and BVL-2. Power system data was collected every 2 minutes for one complete orbit. This data established the baseline operating condition with which the power boost operation was compared. Then without altering any spacecraft loads or orbit parameters, the power boost routine was enabled and data collected real time. Because real time contacts were limited to approximately 10 minutes each, a number of passes over various ground stations were necessary in order to obtain data for a complete orbit.

Analysis and Results

1. Solar Array

The output characteristics of the radiation detector, the auxiliary array and the main array were each analyzed separately to determine solar array degradation. Solar array data collected during orbits 46 (August 24, 1972; third day in orbit) and 44,048 (December 20, 1980; 8 years and 118 days later) is shown in Table 2 and 3. The data shows that EOL array temperatures are significantly higher than BOL values. For instance, at start of sunlight plus 9 minutes the average BOL array temperature is 18.4°C compared to the EOL temperature of 36.2°C. This higher temperature is probably the combined result of coverslide and adhesive darkening and cell efficiency losses.

In order to make comparison of BOL and EOL data, array currents are corrected for temperature differences using the proper short circuit current temperature coefficient. One estimate of 0.050 ma/°C was determined for a similar cell design from Reference 5. Another value was determined using the flight array current and temperature data and fitting the data using a linear regression method. Analysis of BOL data from four paddles shows an average temperature

coefficient of 0.065 ma/°C. Figure 4 shows BOL data for the LLO paddle. Similar analysis was performed on the EOL data but because of excessive data scatter the resulting coefficients varied greatly and are not considered reliable. From these considerations, the temperature coefficient of 0.065 ma/°C was selected and used for subsequent analyses.

Radiation Detector Degradation

For orbit 44,058, the degraded detectors generated an average of 4.05 volts at an average temperature of 13.1°C. This corresponds to an individual cell current of 59.47 ma for the 68.1 ohm load. Applying the solar intensity correction factor of 0.967 for the date of the test results in a corrected cell current of 57.50 ma. For orbit 46, the average detector voltage was 4.31 volts at an average temperature of -3.2°C. The individual cell current in this case was 63.29 ma. For the temperature difference of 16.3°C, the adjustment is 1.06 ma resulting in a current of 64.35 ma. Correction for intensity using a factor of 1.02 for the date of measurement yields a current of 65.63 ma. The comparison of corrected data shows a degradation of 8.13 ma or 14.1%.

Main Array Degradation

Because the average spacecraft load was 492 watts for orbit 46 and 460 watts for orbit 44,058, an analysis was made to determine if the change in the array operating point was significant enough to require any additional correction. The operating point for the cells of the main array during orbit 46 is the array voltage of 30.48 volts plus a diode drop of 0.8 volts or 31.38 volts. Therefore, the average individual cell voltage was 0.326 volts. For orbit 44.058, the main array voltage was 29.90 volts, and allowing for the same diode voltage drop, the individual cell voltage was 0.320 volts. Since the change in the operating voltage of the cells in the main array was only 6 mv, any correction would be insignificant in view of the negligible slope of the I–V curve at this voltage and the resolution of the telemetry.

For orbit 46, the average main array voltage was 30.48. Allowing for a 0.8 volt diode drop, the average individual cell voltage was 0.326 volts. This corresponds to a cell current of 62.33 ma. Including the increase of 1.06 ma for the temperature increase of 16.3°C, the adjusted current is 63.39 ma. Assuming equal contribution from each of the 480 cell strings and applying the solar intensity correction factor, the adjusted and corrected main array current for orbit 46 is 31.03

amperes. For orbit 44,058, the degraded array delivered 26.41 amperes. After corrections and adjustment for solar intensity, the current loss is determined to be 5.50 amperes or 17.7%.

Auxiliary Array Degradation

The auxiliary array voltage was not measured directly, but was calculated from the unregulated bus voltage and by assuming a diode drop and line losses caused by an estimated 20 milliohm line resistance from the array terminals to the unregulated bus.

Using the above method, the cell voltage was found to be 0.330 volts for orbit 46 and 0.326 volts for orbit 44.058. The operating points are again slightly different, but require no further correction.

For orbit 46, the auxiliary array voltage was 30.09 volts. The individual cell voltage was 0.330 volts with a corresponding cell current of 62.30 ma. The cell current adjusted by 1.06 ma for the temperature increase is 63.36 ma. Assuming equal contribution from each of the 104 cell strings, applying the solar intensity correction factor results in an adjusted array current for oribt 46 of 6.72 amperes. For orbit 44,058, the degraded auxiliary array delivered 5.72 amperes, after correction and adjustment for solar intensity. Therefore, the loss equals 1.00 amperes or 14.9%.

One highlight of the auxiliary array data is the current imbalance of approximately 0.5 amperes between the two auxiliary paddles. This discrepancy was observed and reported during the mission. This imbalance is probably caused by the loss of one or more cell strings on the right auxiliary paddle.

These calculated current losses may now be compared to the theoretical short circuit losses due to 1 MeV electron fluence. Based on the OAO–3 circular orbit of 740 km and inclination of 35°, the annual equivalent fluence of 3.55×10^{13} 1 MeV electrons per cm^2 was calculated using Reference 5. The calculations assumed infinite backshielding and no losses due to coverglass darkening. Figure 6 illustrates the normalized short circuit current loss vs. electron fluence for a conventional silicon cell similar to the OAO cell design. The theoretical loss is 14.0% for a total 8.3 year fluence of 2.95×10^{14} 1 MeV electrons per cm^2. Losses calculated from flight data vary from 14.1 to 17.7% and are considered in good agreement with the theoretical value. This agreement indicates that most, but not necessarily all, of the degradation observed was due to radiation damage.

Battery Discharge Characteristics

Prior to conducting the end of mission battery discharge tests, Princeton scientists requested a spacecraft orientation which oriented the main telescope toward the sun for the purpose of evaporating surface contaminants. During this maneuver, the batteries continuously discharged from one eclipse period through the following sunlight period and again through another eclipse. It was determined that battery capacity was approximately 9 ampere-hours down to a bus voltage between 21 and 22 volts prior to terminating the test and returning the spacecraft to a more favorable attitude. Following this discharge, the batteries were allowed to recharge for several days prior to performing the end of mission battery discharge tests.

The battery discharge tests were performed as described earlier. Data was collected continuously and are shown in Figure 7 for the first test and in Figure 8 for the second test.

The individual battery voltages were within approximately 10 mV of each other while battery currents varied only 0.2 amperes between batteries during the entire discharge test. The results of both tests suggest a voltage plateau at a battery voltage of 22.75 volts or approximately 1.034 volts per cell.

Battery cells from the OAO-3 flight lot were evaluated and life cycled by the Quality Evaluation and Engineering Laboratory at Crane, Indiana. The results and analyses of the initial evaluation and life cycle testing appear in Reference 6 and 7, respectively.

Figure 9 compares the two battery discharge tests with the life cycle data from Crane. Pack 4C was cycled at 15% DOD and 10°C in a simulated low earth orbit regime and completed over 33,000 cycles without cell failure prior to discontinuing the test. The discharge capacity data is shown for cell S/N 559 at several times during the life cycle test. The pre-cycling capacity was approximately 27 ampere-hours to a cell voltage of 1.00 volts. As a result of cell aging, the discharge voltage characteristics change significantly as seen by later capacity discharges. Of major importance is the existence of the second voltage plateau apparent during the capacity measurement on cycle 33,298 which is similar to that observed during the OAO-3 discharge tests. The

average battery capacity measured for the first test was 7.3 ampere-hours to 1.04 volts per cell and 10.0 ampere-hours to 1.03 volts per cell for the second discharge test.

On-Board Processor/Power Boost Regulation

Initial Evaluation

During the first trial of the power boost mode, the power boost routine was energized for only the first 12 minutes of sunlight to verify the operation of the worker and power subsystems components. Figure 10 illustrates the array power which the OBP calculates every 6 seconds prior to shifting the duty cycle of the PRU to maintain array power at 900 watts. Figure 11 shows the measured array voltage during the same period.

For the first 3 minutes, the array operating point varies as much as 250 watts above and below the software limit and gradually drops off due to the loss of array power with increasing temperature. The slope of array power vs. time is an indication of the rate at which the array power curve shifts due to array heating. Three minutes into the sunlight, the calculated array power falls below 900 watts causing the OBP to alter the array operating point above 900 watts. This condition occurs again 6 minutes after sunrise. OBP control is terminated after 9 minutes when the battery voltage reaches the battery voltage limit.

Final Evaluation

The final test required collecting power system data for one complete orbit prior to and after enabling the power boost worker. Figures 12 through 15 represent array and battery data during one complete orbit starting with the eclipse period for both the baseline condition (Figures 12 and 13) with the power system in the shunt mode (PRU by-pass relay closed) and in the power boost mode (Figures 14 and 15) with the OBP in control of the PRU (by-pass relay open). The orbit period is approximately 98 minutes long with 35 minutes eclipse and 63 minutes sunlight. In the shunt mode, array power is limited because the array voltage is clamped to the battery voltage (Figure 12). As seen in Figure 13, individual battery currents remain within 0.1 amperes

of each other throughout the orbit. During the initial sunlight period, battery charge currents are limited to approximately 4 amperes. After 34 minutes in sunlight, the battery voltage reaches the voltage limit and triggers the BVL controller to adjust the PRU to maintain the battery voltage level. The average end of light battery current is approximately 0.83 amperes. The battery charge-to-discharge ampere hour ratio (C/D) is 1.02. The end of light battery temperature is approximately 7.9°C.

With the power boost enabled and the OBP array limit set to 1300 watts, the OBP will automatically attempt to adjust the PRU to track the maximum array power (Figure 14). The initial battery charge currents (Figure 15) are approximately 6 amperes. After 21 minutes of sunlight, the OBP releases control to the BVL controller as the battery charge currents taper to an average of 0.7 amperes. The battery recharge ratio (C/D) is approximately 1.05 and the end of light battery temperature is 8.7°C.

There are significant differences in the operation of the power subsystem between the shunt mode and the OBP array power tracking mode. Because the PRU regulates to the maximum array power point when power boost is enabled, more array power is available to recharge the battery resulting in higher initial battery charge current. With this, the battery voltage reaches the BVL in less time than in the shunt mode, resulting in higher percent recharge and temperature. Figure 16 shows array power vs. time since sunrise for both the shunt mode and the power boost mode. The array power shown for the power boost trial represents maximum and minimum excursions around the peak power point to which the OBP has adjusted the PRU. The additional array power available in the power tracking mode is the difference between the array power in the shunt mode and the power boost mode.

Table 4 summarizes the final OBP power boost evaluation compared to the pre-flight performance determined during acceptance thermal vacuum testing (ATV). While a direct comparison between pre-flight and end of mission performance is difficult, the higher initial and average battery charge current and greater percent recharge using the power boost mode indicates successful array power tracking by the OBP/PRU.

CONCLUSIONS AND RECOMMENDATIONS

The end of mission power subsystem engineering analysis provided significant information on the degraded power subsystem components. Specific conclusions are:

1. Solar Array

   a. Current degradations were found to be (1) radiation detector, 14.1%; (2) main array, 17.7%; and (3) auxiliary array, 14.9%.

   b. These degradations are in good agreement with theoretically calculated losses.

   c. Observed degradations are almost entirely due to radiation damage, but there is evidence of additional degradation due to thermal cycling.

2. Battery Discharge Characteristics

   a. The existence of second voltage plateau at approximately 1.03 volts per cell was confirmed.

   b. Degraded voltage characteristics are in close agreement with laboratory life cycle simulations.

   c. Life cycle simulations provide an accurate data base for mathematical modeling of cell lifetime.

   d. Limited pre-flight testing of flight batteries during spacecraft integration contributed to trouble-free battery performance.

3. OBP/Power Boost Regulation

   a. Maximum array power trackers provide increased system utilization by providing (1) additional energy to recharge the battery or for increased load capability and (2) increased flexibility in science data collection.

   b. Operation of nickel-cadmium batteries in parallel through a single charger was demonstrated.

ACKNOWLEDGEMENTS

The author acknowledges the contributions of Michael Malison, Harry Wajsgras, and David Lozinsky of the Grumman Aerospace Corporation for their assistance during the end of mission power subsystem tests; Luther Slifer of the Goddard Space Flight Center for technical support in analyzing the data; and Terry Schmitt and William Anderson of the OAO Corporation for their help in reprogramming the OBP.

REFERENCES

1. "OAO Battery and Power System Design," F.E. Ford, 1977 Battery Workshop CP 2041, Nov. 15–17, 1977.

2. "OAO Functional Operations Manual, Power Subsystem," Document Number FO–G–0217–C, Vol. F, August 1972.

3. "OAO Functional Operations Manual, On-Board Processor (OBP)," Document Number FO–G–0127–C, Vol. F, August 1972.

4. "Low Cost Modular Spacecraft," NASA/GSFC, X–700–75–140, May 1975.

5. "Solar Cell Radiation Handbook," H. Tada and J. Carter, TRW Systems Group, Rendondo Beach, California, November 1, 1977, NAS–7100.

6. "Initial Evaluation Tests, 20AH Nickel–Cadmium Spacecraft Cells," QEEL/C 73–459, December 3, 1973.

7. "Ninth through Fifteenth Annual Report of Life Cycle Test," 1973 through 1979, Quality Evaluation Laboratory, NAD Crane, Indiana.

Table 1
OAO–3 Nickel–Cadmium Cell Design Features

Cell Manufacturer:	Gulton	
Cell Capacity:	20 AH Nominal	
Separator:	Pellon 2505	
Electrolyte:	34% KOH 66 CC	
	Positive Plate	Negative Plate
Number	9	10
Area	0.91 dm^2	0.91 dm^2
Thickness	0.8763 mm	0.7849 mm
Porosity	46.7%	66.5%
Plate Loading	16.1 gr/dm^2	16.95 gr/dm^2
Capacity/Area	4.12 AH/dm^2	4.20 AH/dm^2
Flooded Capacity	27.7 AH	39.8 AH*

*Capacity measured to -1.0V.

Table 2
Beginning of Mission Solar Array Characteristics

Orbit 46		B = 58		θ = 0		BVL = 1		Day 237			T Bat = 10°C	
Time in Orbit	Set	Unreg. Bus Curr. (0-59)	Conv. Input Curr. (E-57)	Total Bus Curr. (Amps)	Unreg. Bus Volt (D-29) (Volts)	Unreg. Bus Load (Watts)	Array LLO Curr. (0-05)	Array LRA Curr. (0-18)	Total Aux. Array Curr. (Amps)	Rad. Det. LRI (0-31)	Rad. Det. LLI (E-44)	Avg. Rad. Det. Volts
L+0 min.	6137											
L+1 min.	6134	8.22	8.98	17.2	28.18	484.7	3.30	3.31	6.61	4.27	4.19	4.23
L+2 min.	6147	8.14	8.82	17.0	28.58	485.9	3.32	3.33	6.65	4.27	4.19	4.23
L+3 min.	6153	8.06	8.82	16.9	29.04	490.8	3.34	3.35	6.69	4.27	4.21	4.24
L+4 min.	6157	8.06	8.82	16.9	28.97	489.6	3.40	3.39	6.79	4.31	4.25	4.28
L+5 min.	6163	8.13	8.74	17.1	29.11	497.8	3.42	3.41	6.83	4.33	4.29	4.31
L+6 min.	6167	7.98	8.74	16.7	29.50	492.7	3.44	3.45	6.89	4.37	4.31	4.37
L+7 min.	6173	8.14	8.66	16.8	29.17	490.1	3.46	3.46	6.92	4.37	4.33	4.35
L+8 min.	6177	7.98	8.66	16.8	29.50	489.7	3.48	3.49	6.97	4.39	4.35	4.37
L+9 min.	6203	8.31	8.58	16.9	29.90	505.3	3.46	3.47	6.93	4.39	4.35	4.37
L+10min.	6207	7.90	8.58	16.5	29.90	493.4	3.46	3.46	6.92	4.37	4.35	4.36
Avg of 10					29.16	492.0	3.41	3.41	6.82	4.33	4.28	4.31

Time in Orbit	Set	Array Volts (D-30)	Array UL Curr. (E-13)	Array UR Curr. (E-39)	Array LLI Curr. (E-26)	Array LRI Curr. (E-52)	Total Main Curr. (Amps)	Array Temperatures (°C) LLI (B-16)	URI (A-19)	LLO (A-1)	URO (A-33)	Avg. Array Temp (°C)
L+0 min.	6137											
L+1 min.	6143	29.37	9.26	9.19	6.26	6.27	30.98	-40.2	-32.6	-41.5	-34.5	-37.2
L+2 min.	6147	30.10	9.44	9.25	6.30	6.31	31.30	-33.5	-21.5	-29.2	-21.5	-26.5
L+3 min.	6153	30.10	9.57	9.31	6.38	6.35	31.61	-29.2	-12.6	-21.0	-11.7	-18.7
L+4 min.	6157	30.10	9.57	9.43	6.42	6.43	31.85	-22.7	- 4.9	-13.9	- 4.2	-19.7
L+5 min.	6163	30.58	9.69	9.49	6.50	6.47	32.15	-17.5	2.9	- 6.1	7.1	- 3.4
L+6 min.	6167	30.58	9.81	9.61	6.54	6.55	32.51	-13.5	9.9	0.6	14.6	2.7
L+7 min.	6173	30.58	9.87	9.67	6.54	6.55	32.63	- 8.7	14.6	6.7	20.6	8.3
L+8 min.	6177	31.05	9.81	9.67	6.58	6.59	32.65	- 3.1	19.2	12.5	26.5	13.7
L+9 min.	6203	31.06	9.87	9.67	6.62	6.59	32.75	1.3	23.7	17.1	31.4	18.4
L+10min.	6207	31.30	9.81	9.61	6.58	6.55	32.55	5.7	27.0	20.3	35.2	22.0
Avg of 10		30.48	9.67	9.49	6.47	6.47	32.10					- 3.2

Table 3
End of Mission Solar Array Characteristics

Orbit 44058		B = 57°		θ = 0	BVL = 1		% Sun = 65%		Day 355		T Bat = 9.4°C	
Time in Orbit	Set	Unreg. Bus Curr. (0–59)	Conv. Input Curr. (E–57)	Total Bus Curr. (Amps)	Unreg. Bus Volt (D–29)	Unreg. Bus Load (Watts)	Array LLO Curr. (0–05)	Array LRA Curr. (0–18)	Total Aux. Arr. Curr. (Amps)	Rad. Det. LRI (0–31)	Rad. Det. LRE (E–44)	Avg. Rad. Det. (Volts)
L+1 min.	2454	7.74	8.90	16.64	28.38	472.2	3.13	2.64	5.77	4.01	3.81	3.91
L+3 min.	2464	7.66	8.82	16.48	28.51	469.8	3.19	2.66	5.85	4.09	3.89	3.99
L+5 min.	2474	7.66	8.74	16.40	28.64	469.7	3.28	2.70	5.98	4.17	3.97	4.07
L+7 min.	2504	7.58	9.06	16.64	29.24	496.5	3.30	2.72	6.02	4.23	4.05	4.14
L+9 min.	2514	6.14	8.98	15.12	29.30	443.0	3.32	2.70	6.02	4.23	4.07	4.15
Avg of 5					28.81	468.2	3.24	2.68	5.92	4.14	3.95	4.05

Time in Orbit	Set	Array Volt (D–30)	Array UL Curr. (E–13)	Array UR Curr. (E–39)	Array LLI Curr. (E–26)	Array LRI Curr. E–52)	Total Main Array Curr.	Array Temperatures (°C) LLI (B–16)	URI (A–19)	LLO (A–1)	URO (A–33)	Avg. Array Temp. (°C)
L+1 min.	2454	29.37	7.93	8.34	5.45	5.58	27.30	-24.4	1.3	-24.4	—	-15.8
L+3 min.	2464	29.37	7.99	8.34	5.33	5.54	27.20	-10.4	21.4	- 6.1	—	1.6
L+5 min.	2474	30.10	7.99	8.40	5.45	5.54	27.38	3.3	35.7	9.3	—	16.1
L+7 min.	2504	30.34	7.99	8.52	5.37	5.58	27.46	14.6	46.5	21.4	—	27.5
L+9 min.	2514	30.34	7.99	8.46	5.29	5.54	27.28	24.1	53.6	30.9	—	36.2
Avg of 5		29.90	7.98	8.41	5.38	5.55	27.32					13.1

Table 4
OBP Power Boost Evaluation Summary

Parameter	Pre-Flight Measurement		End of Mission Test Data	
	Without Power Boost	With Power Boost	Without Power Boost	With Power Boost
Orbit(s)	ATV[1]	ATV	44,703	44,744 to 44,756
Beta	15	15	90	90
BVLS	4	4	2	2
Discharge AH	3.85AH	3.85AH	3.3AH	3.3AH
Battery EOD [2] Voltage	27.25 V	27.35V	26.15V	26.28V
Battery EOC[3] Current	2.0 AMP	0.9 AMP	0.83 AMP	0.66 AMP
Battery EOC Temp.	9.2°C	10.2°C	7.9°C	8.7°C
Percent Recharge	103%	105%	102%	105%
Battery SOL [4] Current	4.3 AMP	6.2 AMP	3.2 AMP	6.0 AMP
Battery Current Prior to BVL	4.0 AMP	4.5 AMP	3.9 AMP	4.2 AMP
Average Battery Current from SOL to BVL	4.2 AMP	5.0 AMP	3.8 AMP	4.8 AMP

[1]Acceptance thermal vacuum testing.
[2]End of discharge.
[3]End of charge (end of light).
[4]Start of light.

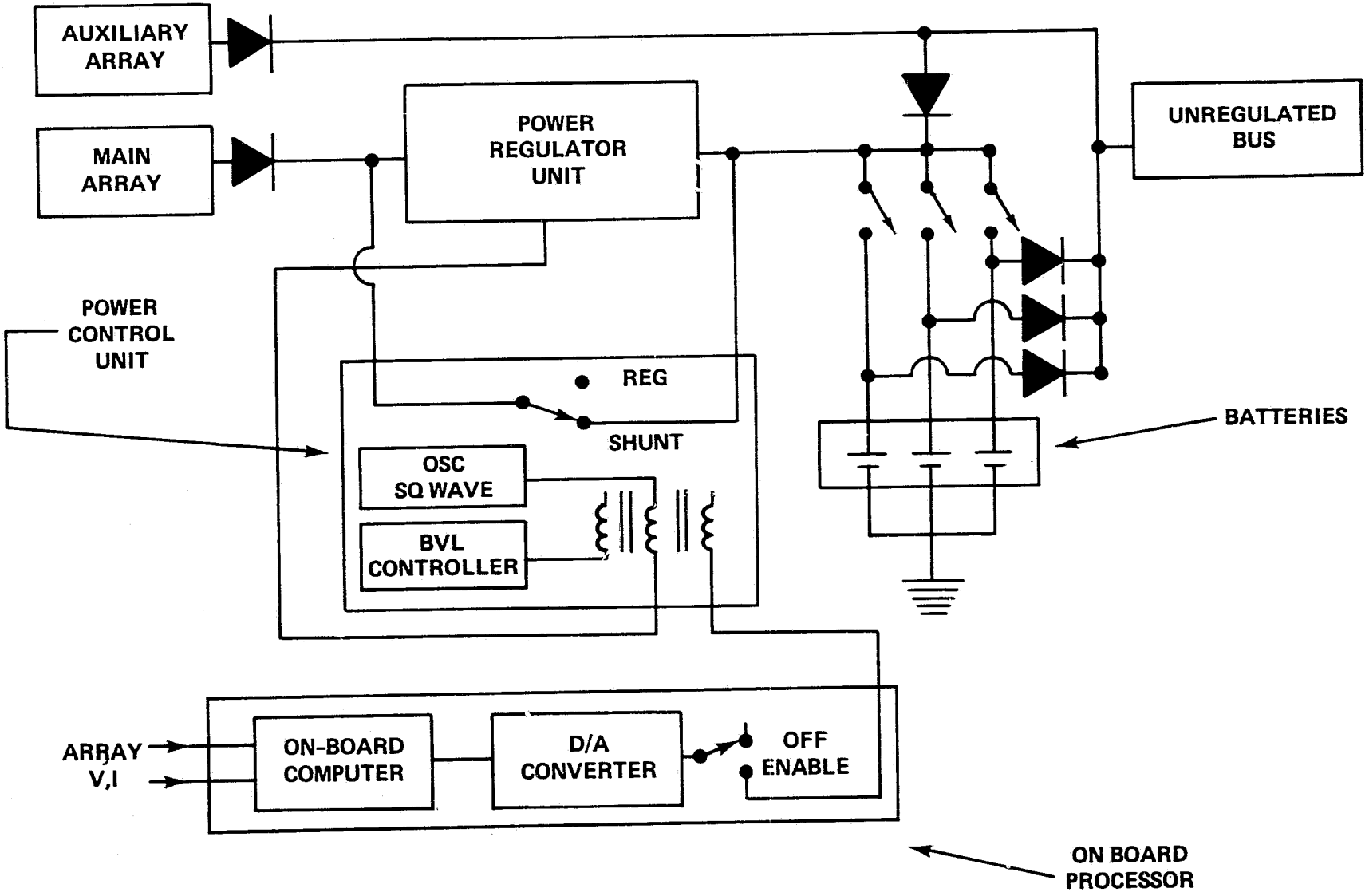

Figure 1. Block Diagram of OAO 3 Power Subsystem.

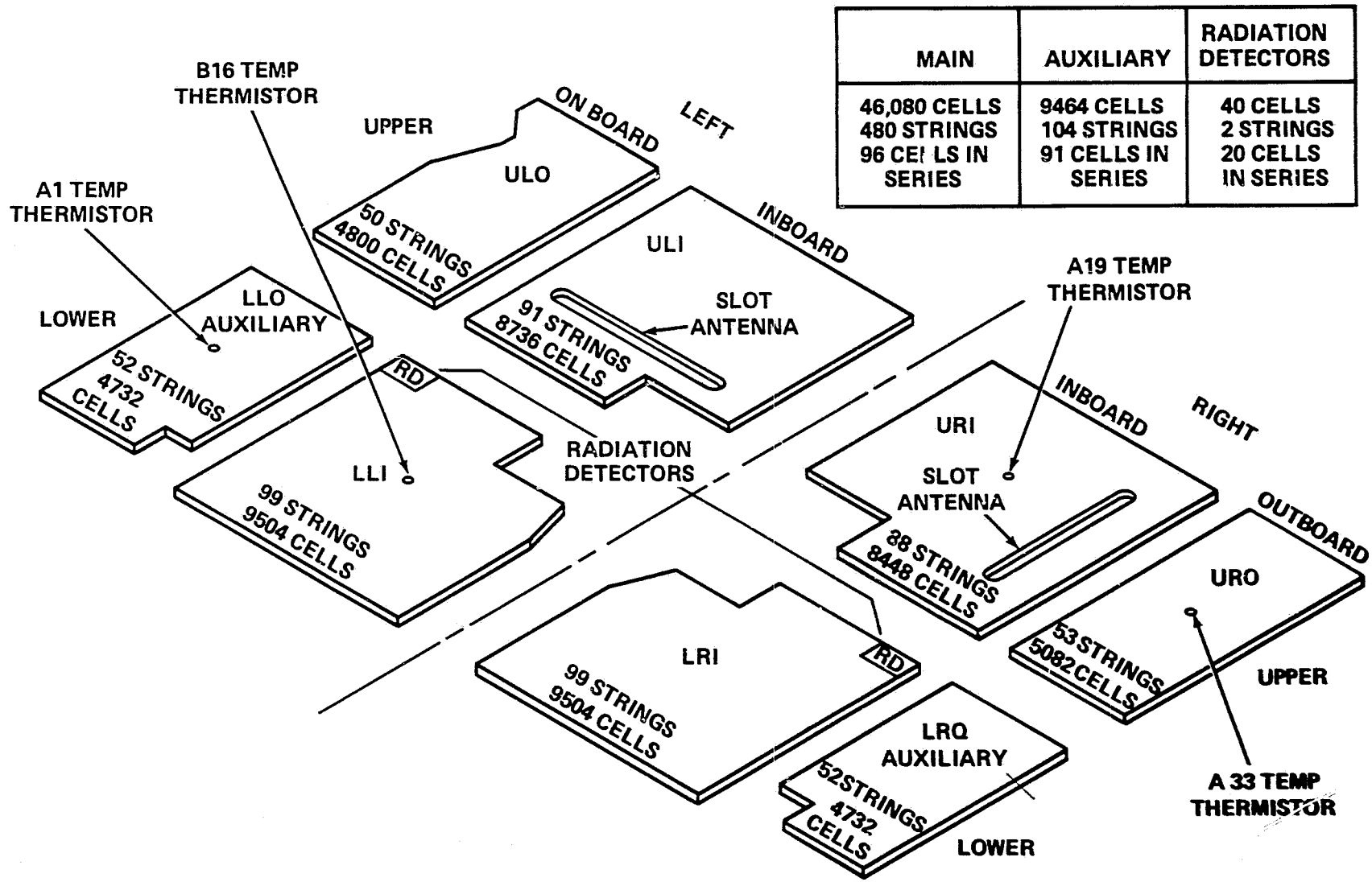

Figure 2. OAO-3 Solar Array Paddle Arrangement.

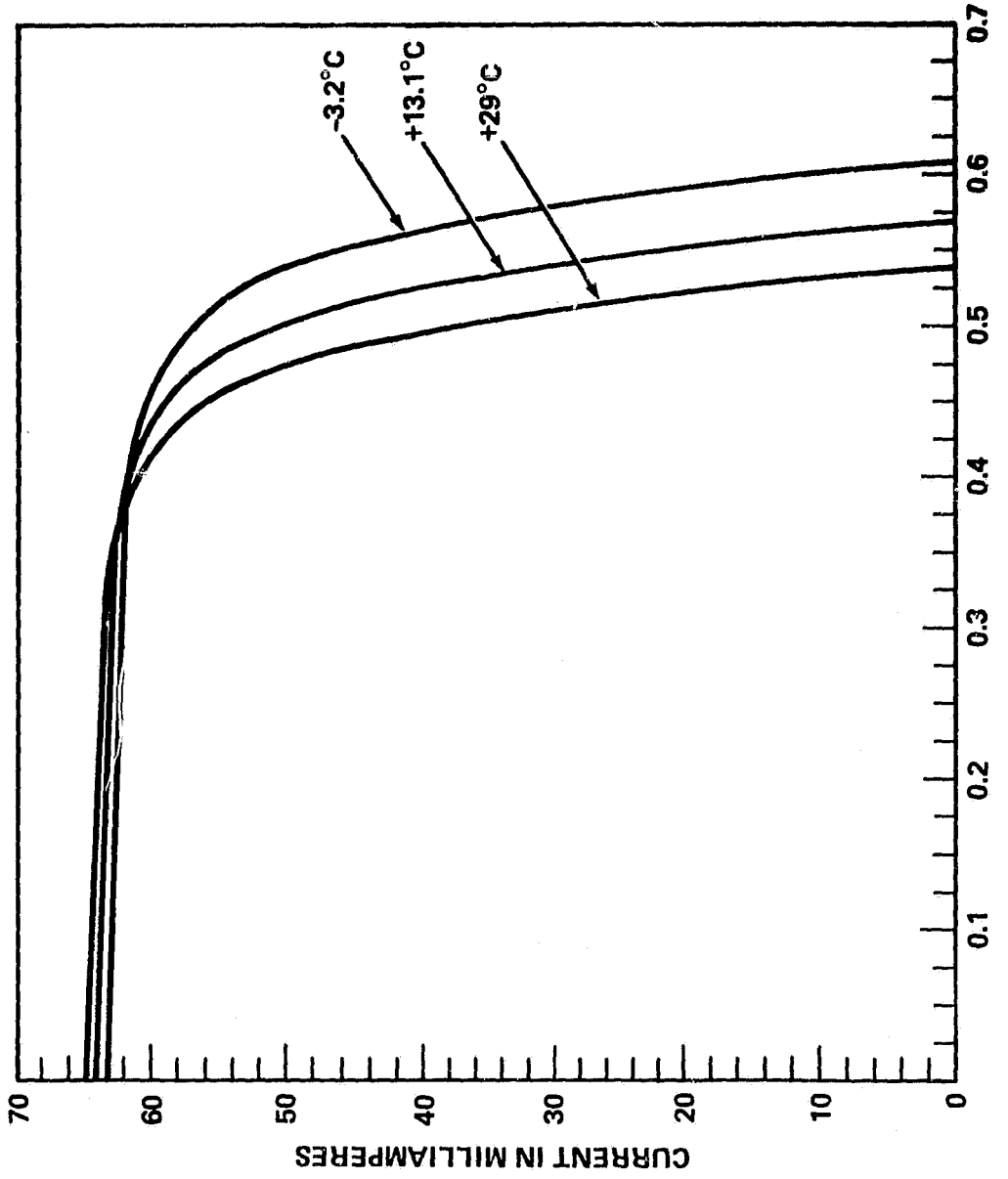

Figure 3. OAO–3 Solar Cell Characteristics (BOL).

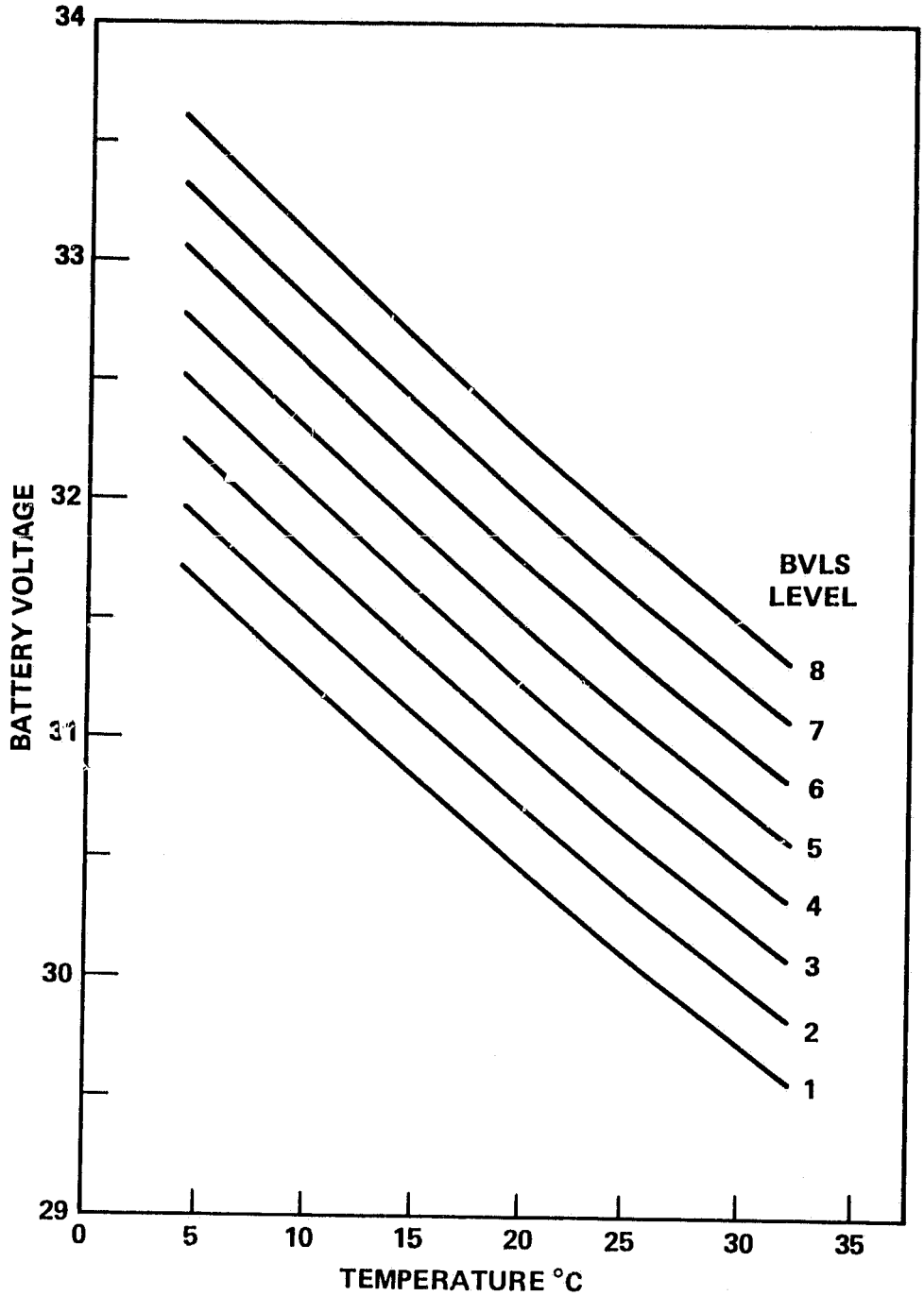

Figure 4. Battery Charger Voltage Levels.

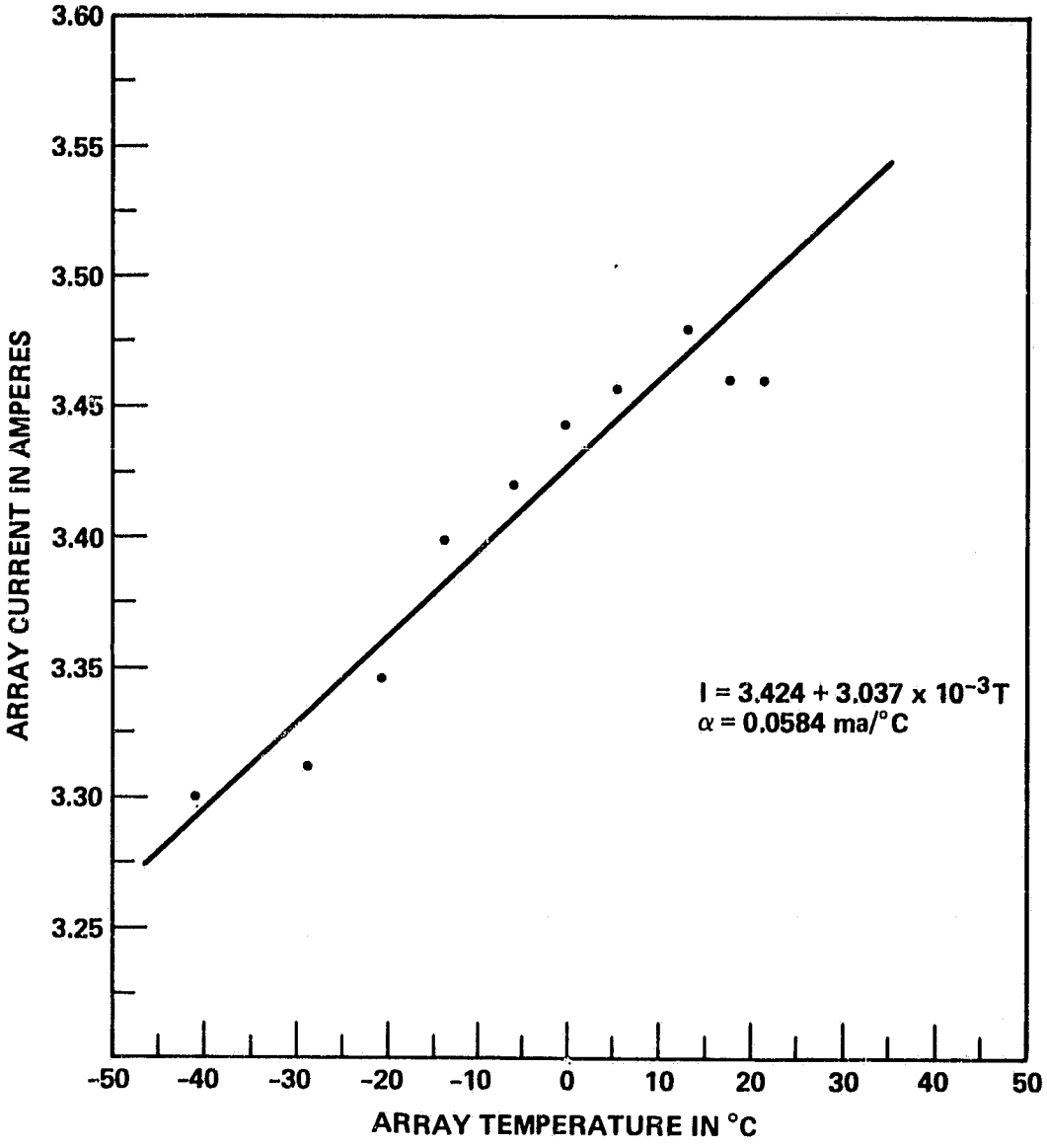

Figure 5. BOL LLO Array Current vs Temperature.

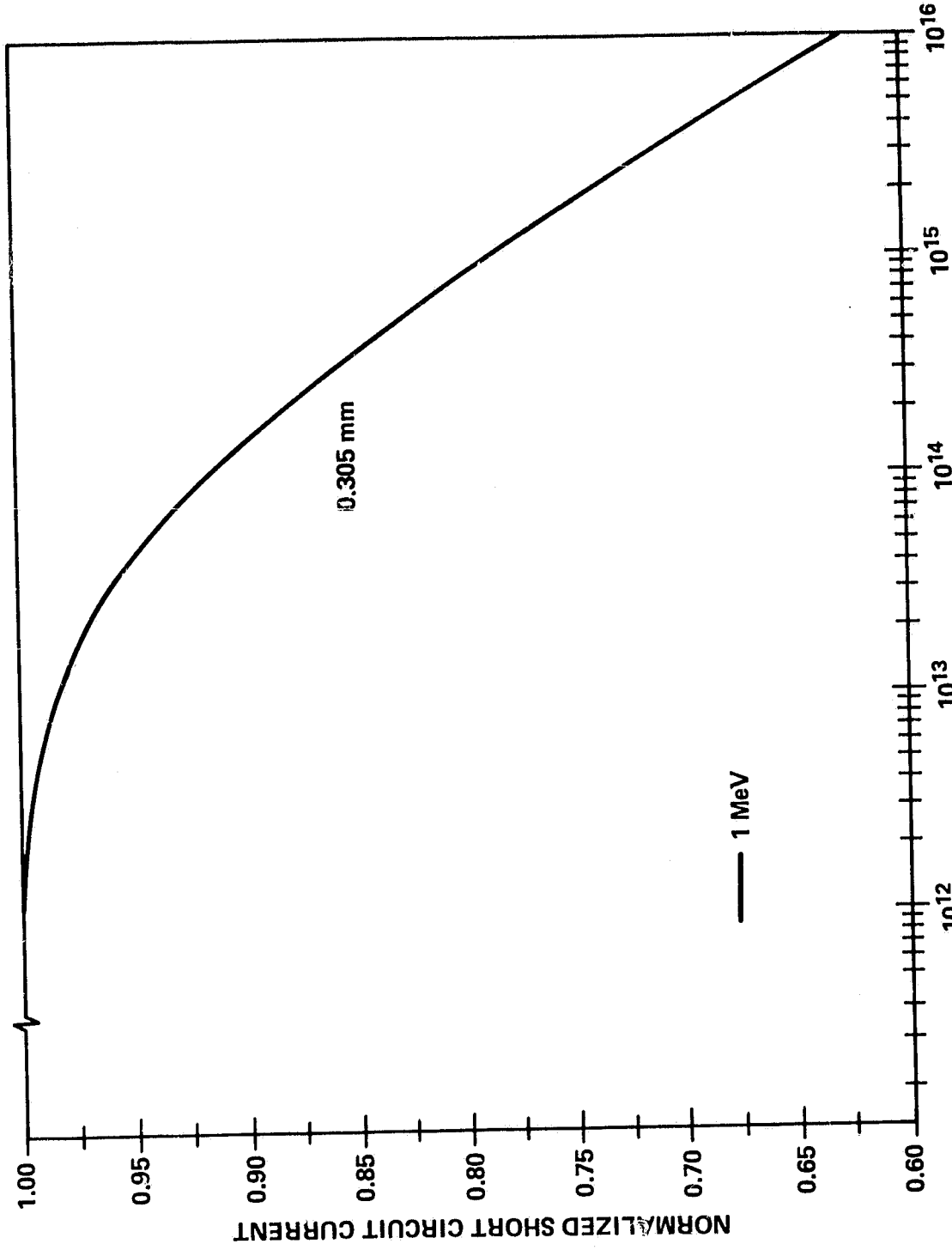

Figure 6. Normalized Short Circuit Current vs 1 MeV Electron Fluence for 2 Ohm-cm n/p Conventional Silicon Cells at 135.3 mW/cm^2 AMO Illumination, 30°C.

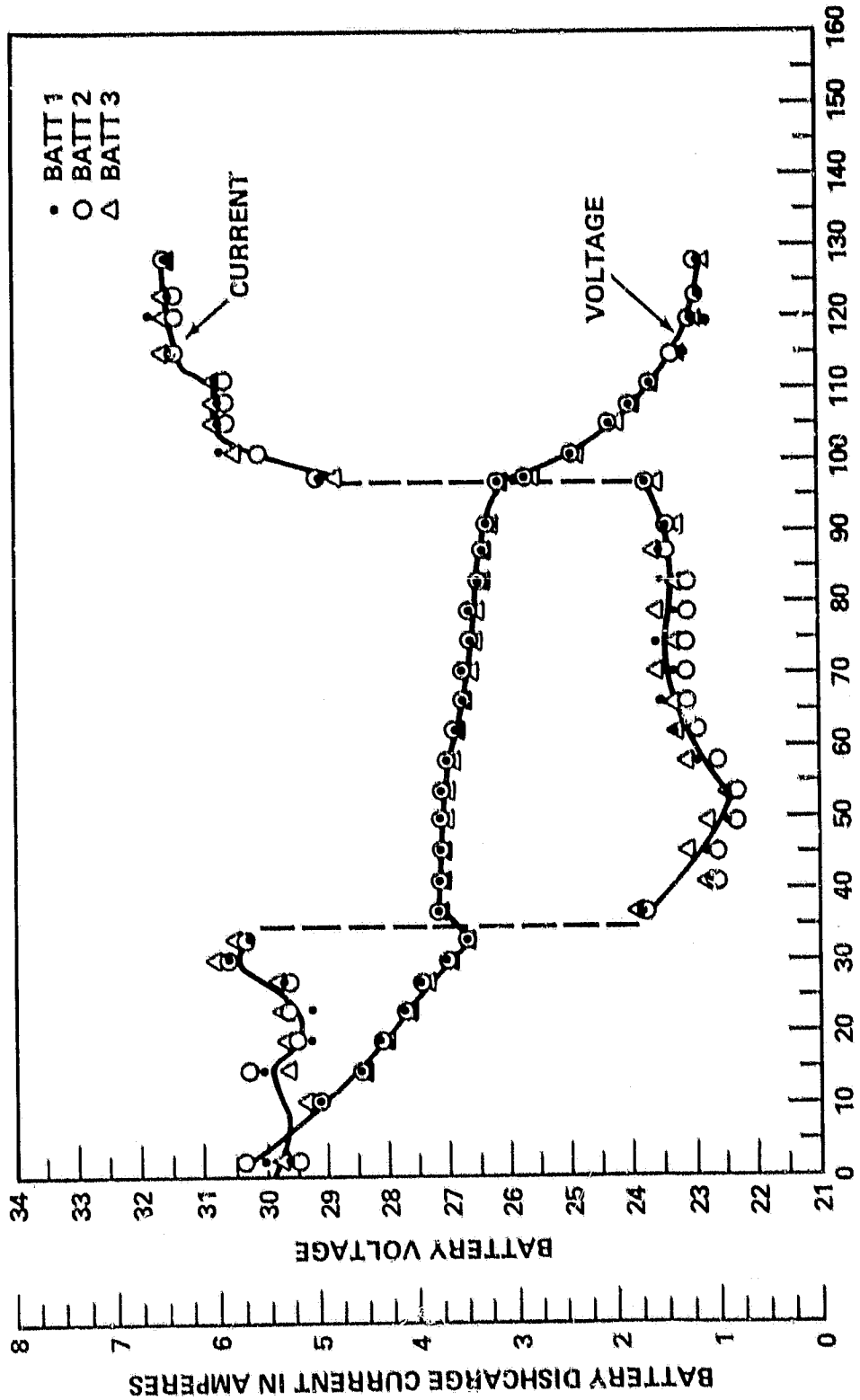

Figure 7. OAO–3 Battery Capacity Discharge Test 1.

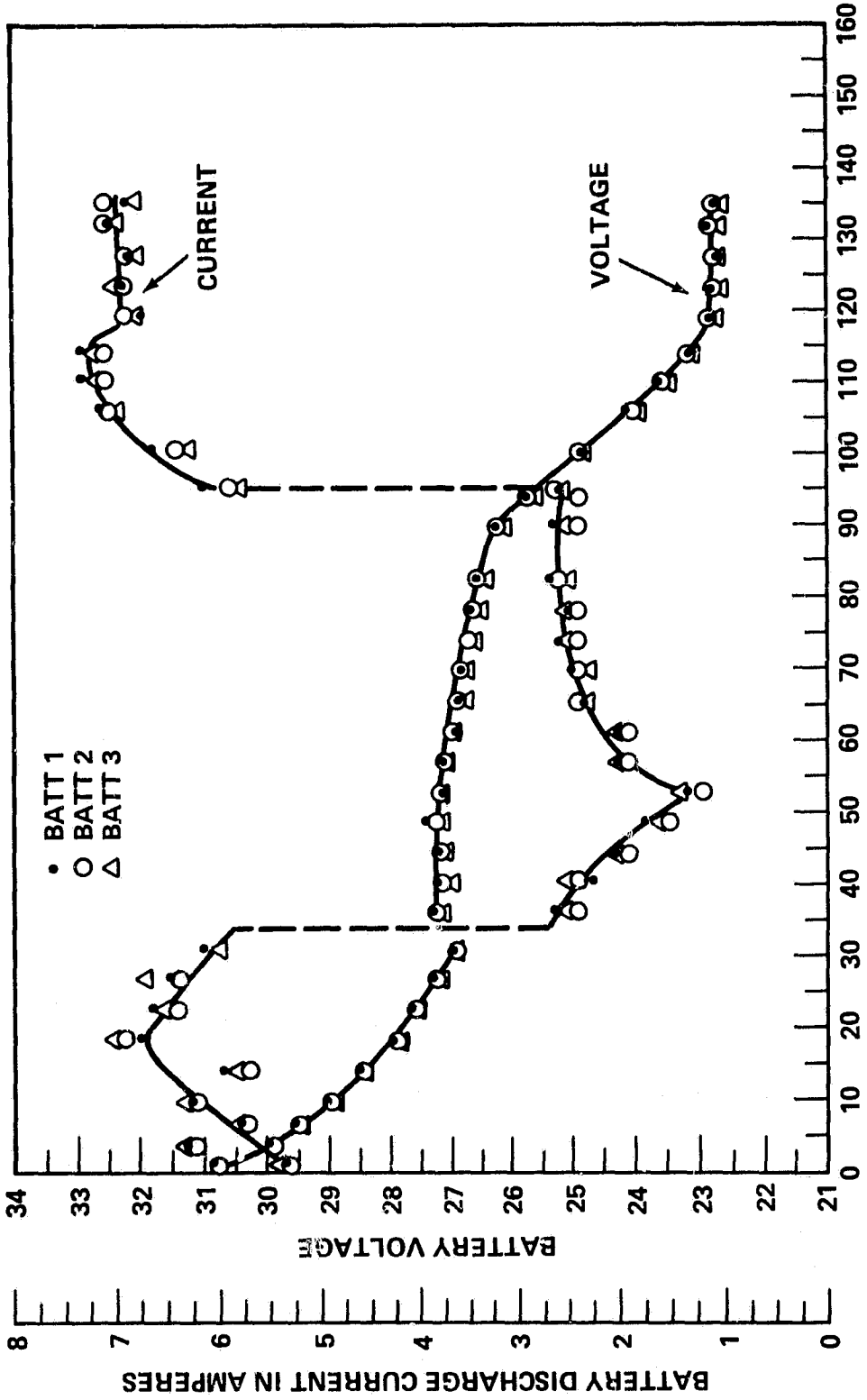

Figure 8. OAO–3 Battery Capacity Discharge Test 2.

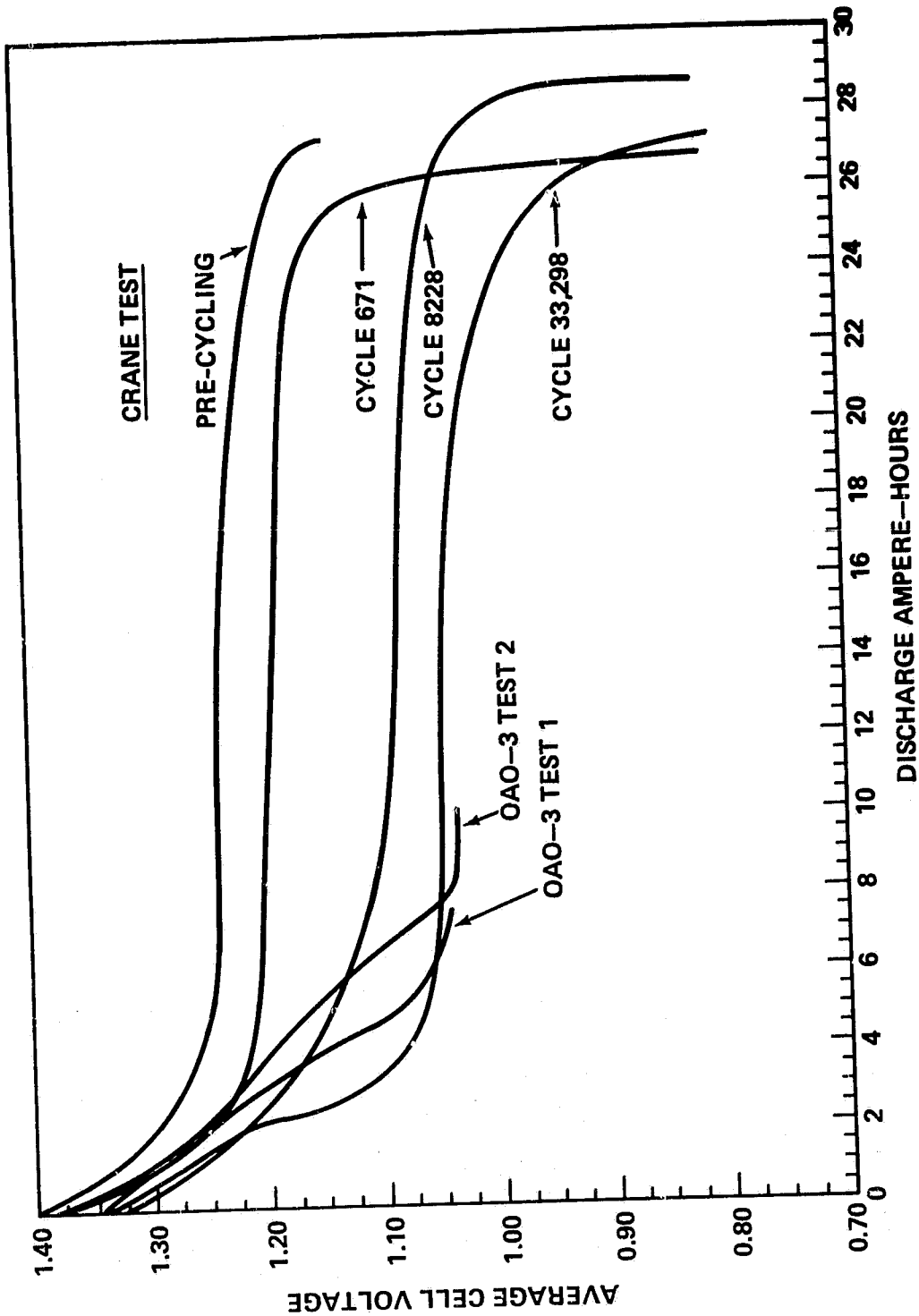

Figure 9. OAO–3 Battery and Crane Discharge, Pack 4c, Cell S/N 559, 15% DOD 10°C.

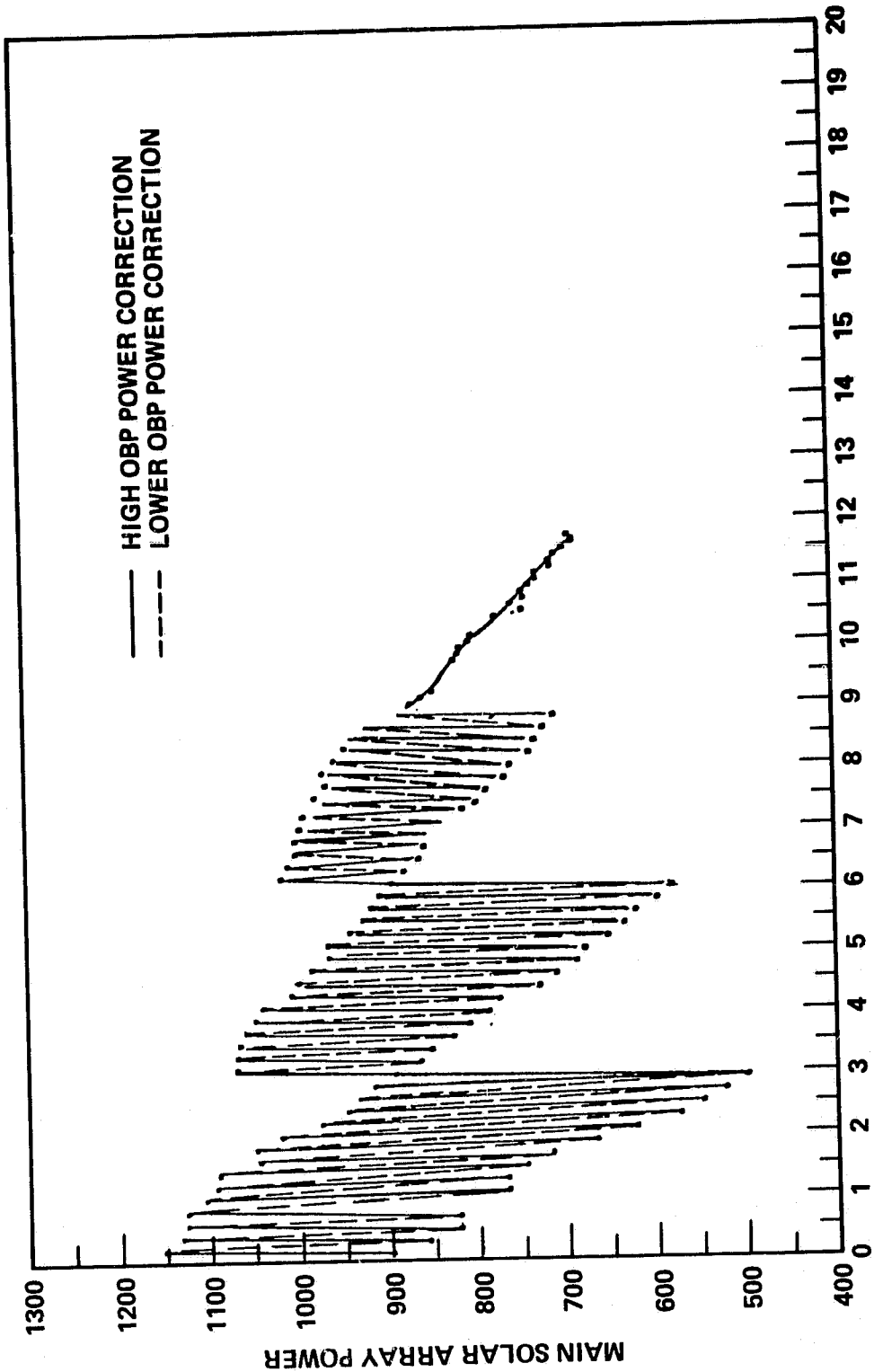

Figure 10. OBP Power Boost Evaluation, Array Power vs Sunlight Time, 900 Watt Power Limit.

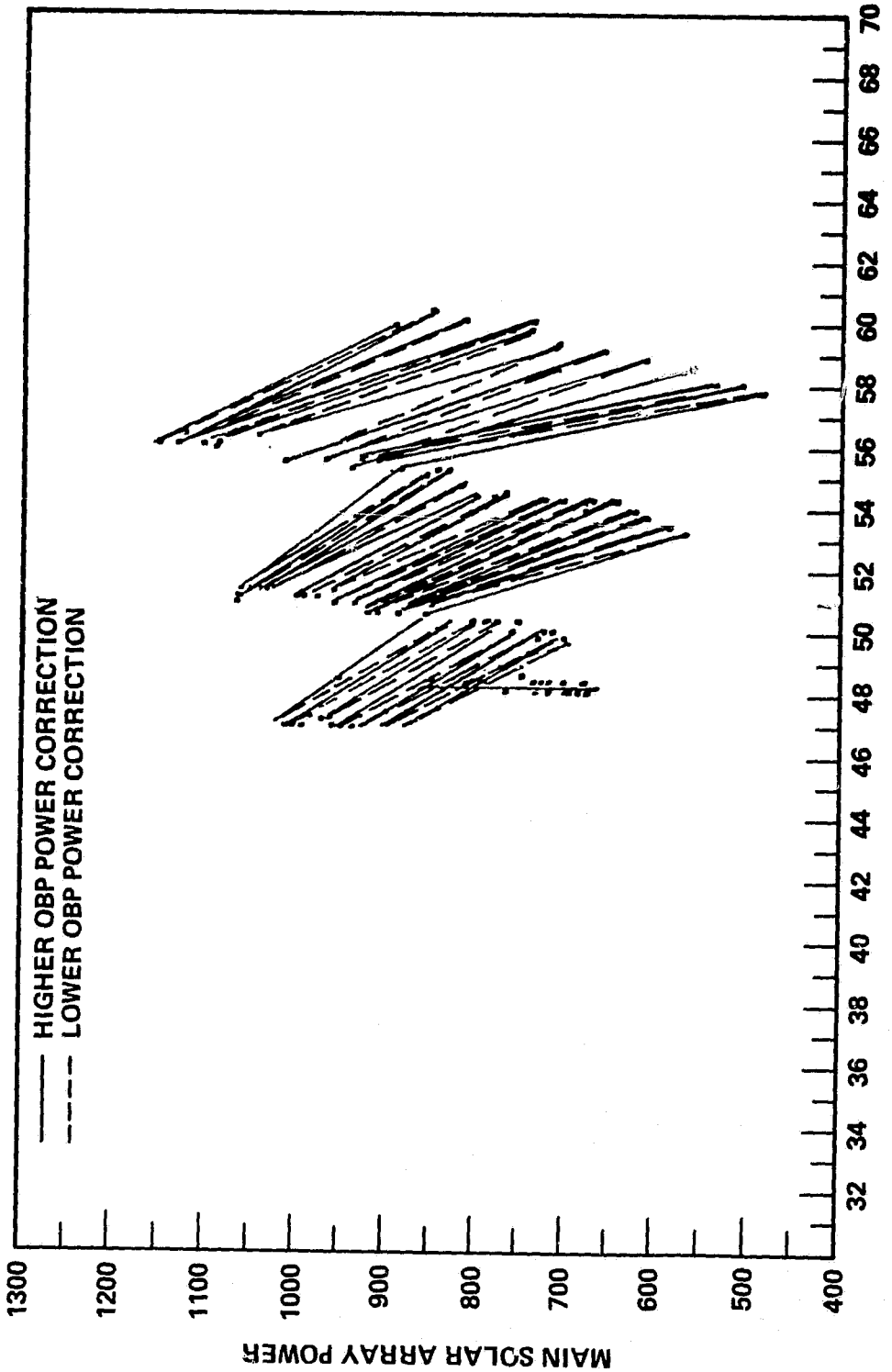

Figure 11. OBP Power Boost Evaluation, Array Voltage vs Sunlight Time, 900 Watts Power Limit.

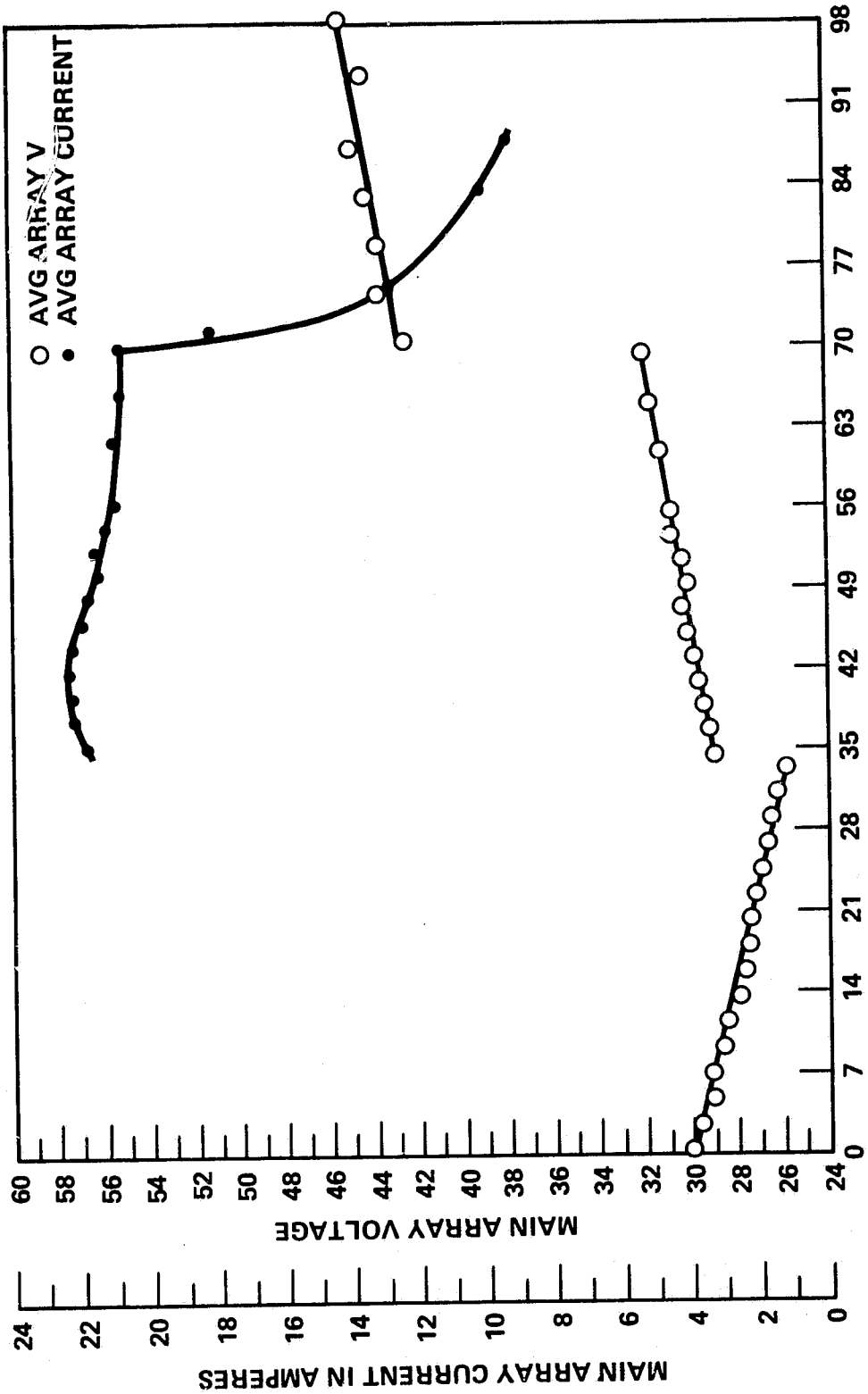

Figure 12. Array Current and Voltage, Shunt Regulation Mode.

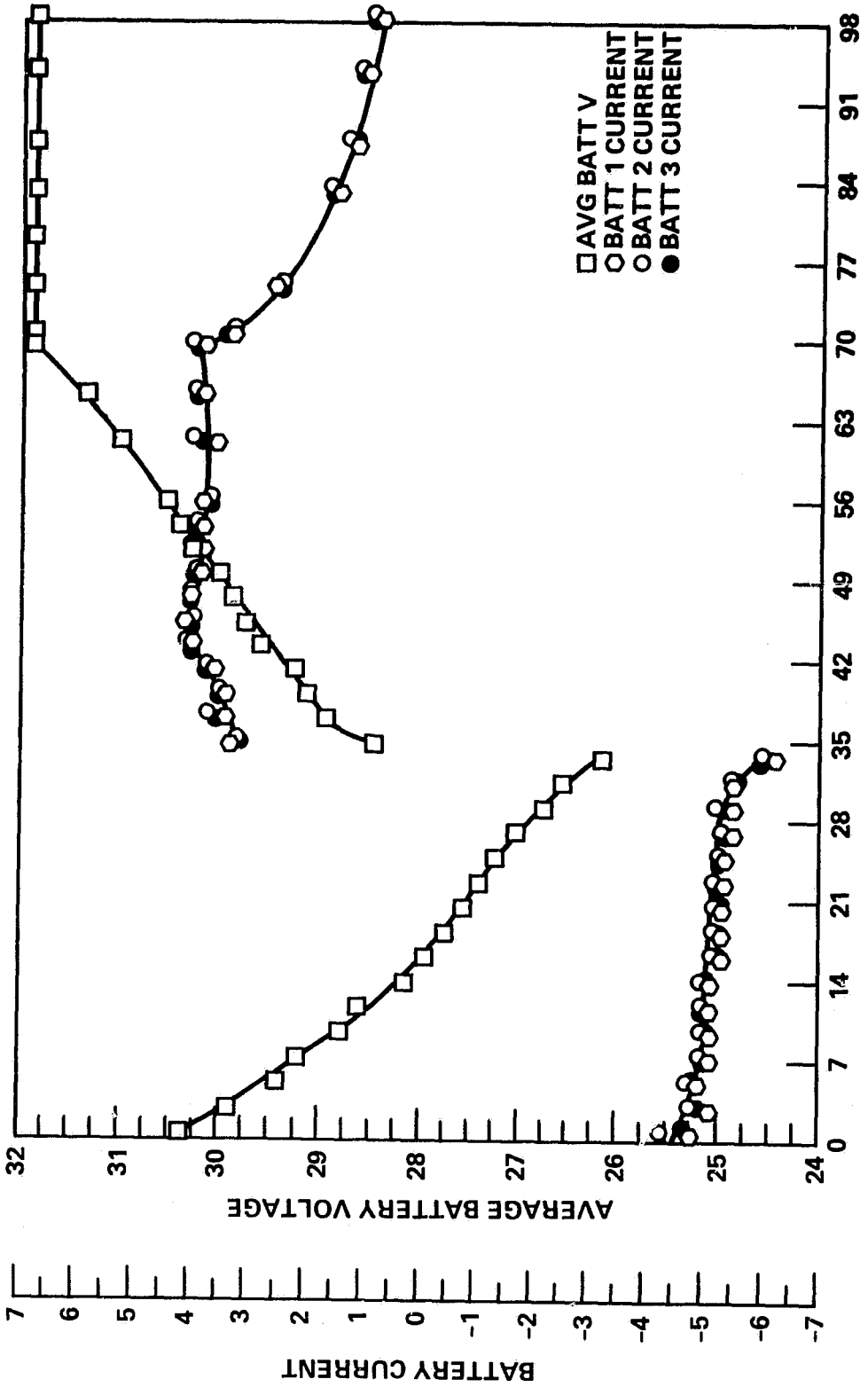

Figure 13. Battery Current and Voltage, Shunt Regulation Mode.

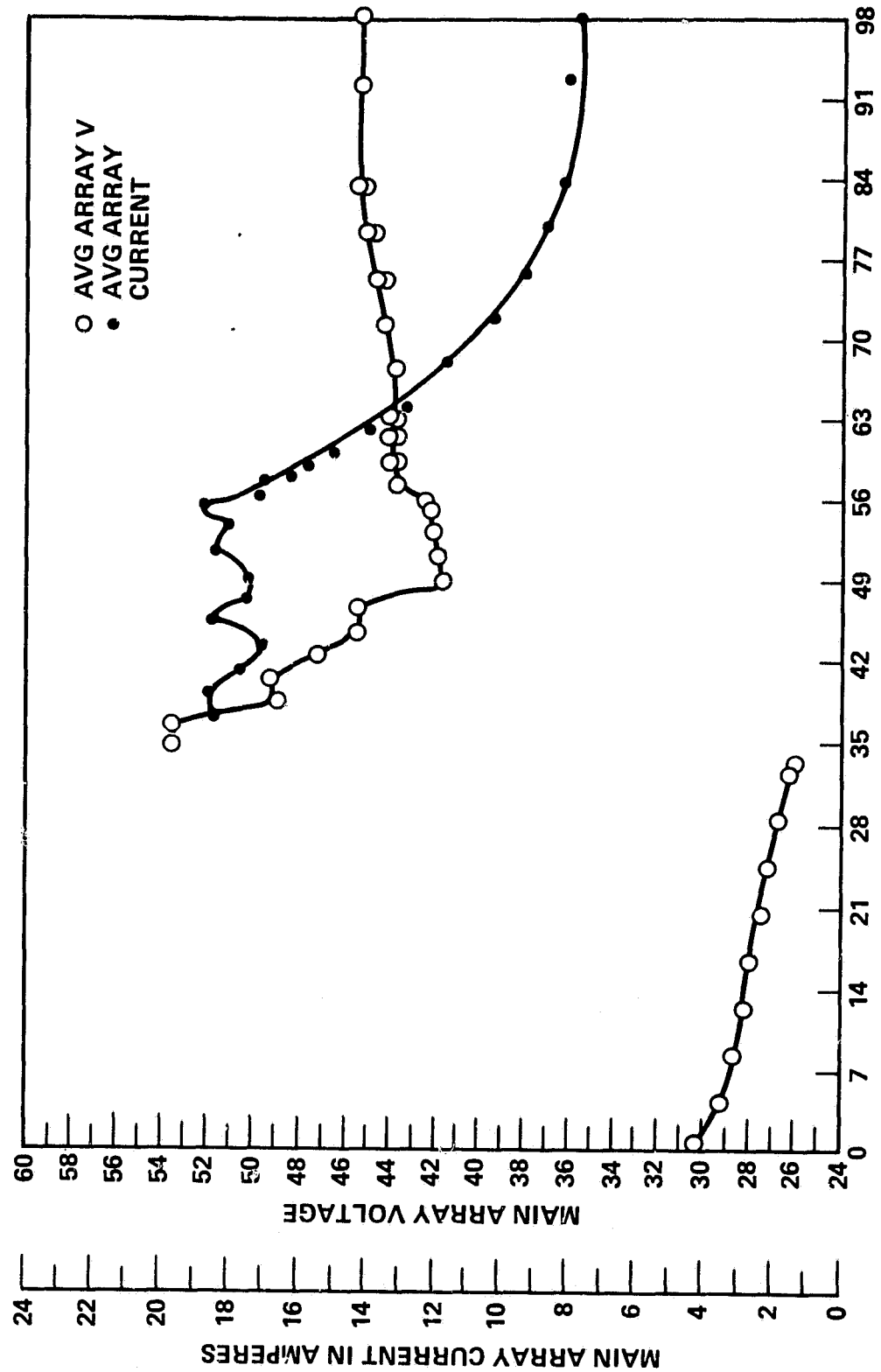

Figure 14. Array Current and Voltage, Maximum Power Tracker Mode.

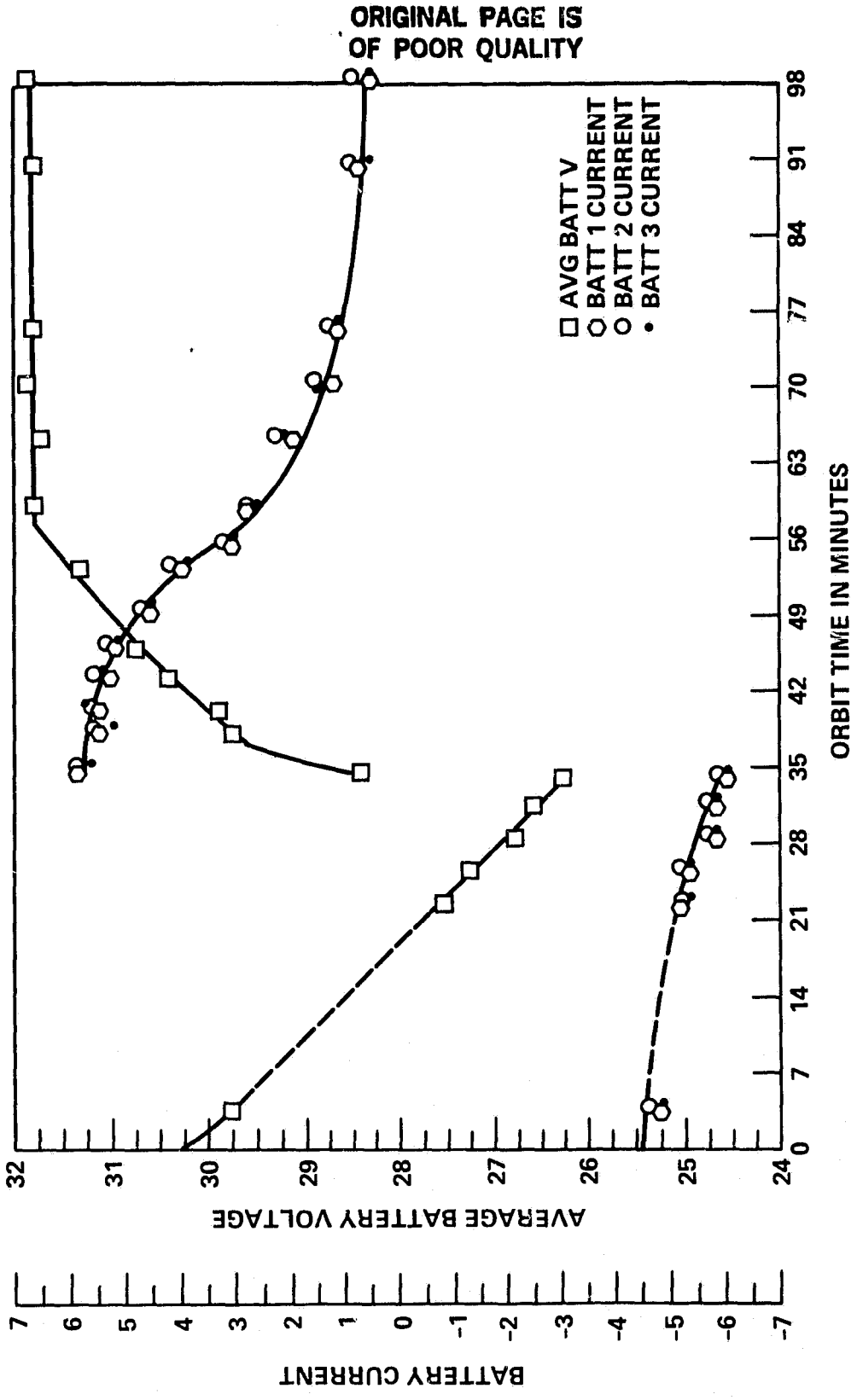

Figure 15. Battery Current and Voltage, Maximum Power Tracker Mode.

ORIGINAL PAGE IS
OF POOR QUALITY

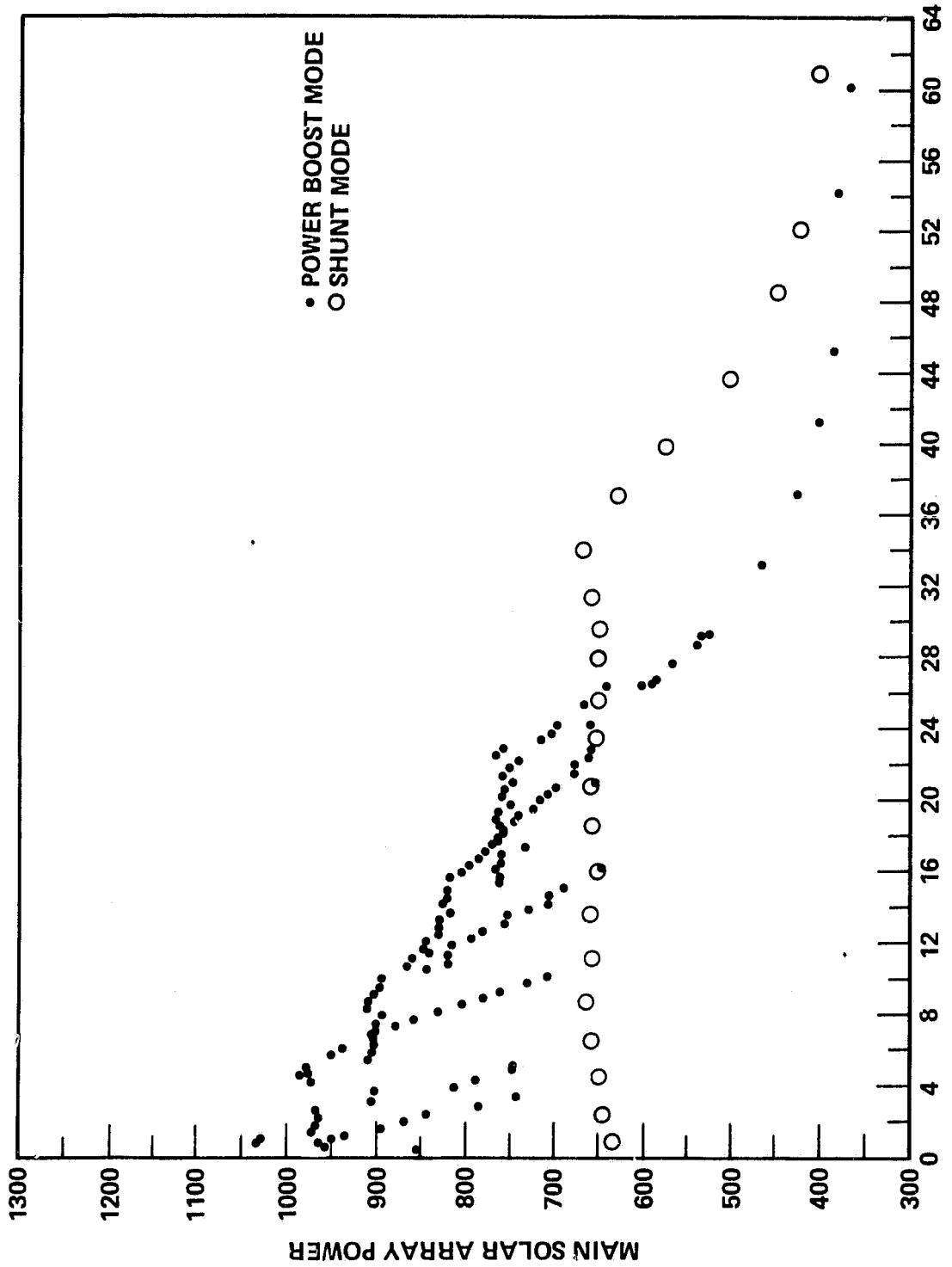

Figure 16. Array Power in Shunt Regulation vs Power Boost Modes.